A Comparative Analysis of XV-15 Tiltrotor Hover Test Data and WOPWOP Predictions Incorporating the Fountain Effect

Charles K. Rutledge
Principal Engineer
Lockheed Engineering and Sciences Company
Hampton, Virginia

Charles D. Coffen
Graduate Research Assistant
Cornell University
Ithaca, New York

Albert R. George
Professor
Cornell University
Ithaca, New York

Abstract

Acoustic measurements from a hovering full-scale XV-15 tiltrotor with the advanced technology blades are presented which show the directionality of "fountain effect" noise. Predicted acoustic directivity results are also presented which show agreement with the measured data. The aeroacoustic code, WOPWOP, was used in conjunction with a mathematical model which simulated the fountain/recirculation aerodynamic effect on the rotors' blade surface pressures. The predictions were used to identify the spike character in the measured data as fountain effect associated noise. The directivity of the fountain effect noise was observed to be dominant at the rear of the aircraft with increased intensities 45 degrees below the rotor disk planes.

Symbols

c	speed of sound, m
r	radial distance from reference coordinate system origin to microphone, m
R	rotor radius, 3.81 m
ρ	air density, kg/m^3
θ	polar angle, angle from reference coordinate system origin to microphone location, negative down
ψ	azimuthal angle in coordinate system reference plane, from zero over tail to microphone location

Abbreviations

obs	observer in far-field
ADDRAS	acoustic division's data reduction and analysis system
ATB	advanced technology blades
BVI	blade vortex interaction
CFD	computational fluid dynamics
Mtip	blade tip Mach number
OASPL	overall sound pressure level, dB
RPM	revolutions per minute

Introduction

Hovering tiltrotor aircraft have a unique noise mechanism which is related to the complex aerodynamics caused by the wings obstructing the downwash from the two rotor systems. The wing establishes a nearby partial ground plane. These aerodynamics are generally characterized (Ref. 1) by a portion of the downwash from each rotor disk (directly above the wings) being diverted inboard after contacting the wings. The flow then collides over the fuselage with a similar flow from the opposite side rotor. The combined flow rises directly above the fuselage, splits and is then entrained into each rotor. This dynamic area of stagnation and subsequent reingestion has been called a fountain-like process. Because the fountain/recirculation phenomenon affects the flow within the disk approximately over the wings, the inflow characteristics associated with the rotor systems are different at these azimuthal stations relative to the remainder of the rotor disk. The resulting noise mechanism, called the "fountain effect", is hypothesized to result from the localized changes on blade loading which result when the blades pass through the area effected by the recirculation.

The fountain's mean flow and its effect at the rotor disk has been found to vary as a

(NASA-CR-189455) A COMPARATIVE ANALYSIS OF XV-15 TILTROTOR HOVER TEST DATA AND WOPWOP PREDICTIONS INCORPORATING THE FOUNTAIN EFFECT (Lockheed Engineering and Sciences Corp.) 20 p

N92-11992

CSCL 01C G3/05

Unclas
0052240

function of time, producing an unsteady blade loading over this portion of the rotor disk. These changing loads effect loading and broadband noise mechanisms. Coffen and George (Ref. 2) have presented noise calculations for discrete frequency and broadband noise which incorporate a "fountain effect" aerodynamic model. One of their results show that the fountain effect associated acoustics have a strongly directional radiation pattern toward the aircraft's rear. Because of limited availability, little experimental data was presented for comparison to these predictions in reference 2.

This investigation was conducted to identify the fountain effect associated acoustic radiation patterns in measured data and to further validate the discrete frequency noise model presented by Coffen and George. Measured data from a recent NASA Langley/Ames far-field acoustics hover test for a full scale XV-15 tiltrotor are used for prediction comparison. The rotor systems on the experimental XV-15 were the Advanced Technology Blades (ATB, Ref. 3) so these were modelled in the theoretical calculations. Previous work with the fountain effect model used the original XV-15 metal blade rotor systems. The purpose of the joint NASA test was to characterize the system noise directivity patterns of an XV-15 tiltrotor in hover mode. These data are ideal for comparisons because this carefully controlled experiment yielded high quality acoustic data allowing high directivity resolution.

The acoustics far-field test was simple in concept to assure quality acoustic data. The test consisted of hovering the XV-15 over a fixed point while remote systems were acquiring data relative to aircraft positioning, local weather and associated acoustics. These data systems are described below.

While the far-field acoustics test design was kept simple, several assumptions about the XV-15 rotor system being modelled were necessary. These assumptions are also described below.

Experimental Setup

Test Location

The hover test was conducted at the Moffett Field Naval Air Station, California, USA. The runway system and research tunnel facilities were on standby for the duration of the acoustics test. The test was performed on three consecutive days in early December, between sunrise and about three hours after. These precautions and timing made the ambient acoustics and weather conditions optimum for the test.

The test area included the northernmost portion of runway 14R-32L and an adjacent field (Fig. 1). A hover point was selected and marked on the centerline of the runway. Microphone locations were accurately determined by surveying techniques every 15 degrees at a constant distance (152.4 m) from the hover point. The adjacent field was flat having primarily two types of vegetation. The vegetation consisted of a tall grass variety and sagebrush, neither of which exceeded 0.5 m in height. Areas close to the microphone locations were cleared of vegetation if it was tall. The mean microphone altitude relative to the hover point was +0.55 meters with a standard deviation of 0.2 meters.

Positioning System

A two theodolite sighting system was used as an aid to position and maintain the XV-15 over the hover point at test altitudes. Two theodolite stations were established approximately 183 m from the hover point at right angles. The theodolite operators were in constant audio and visual contact with the pilot and co-pilot of the XV-15 during hover. By using such contact, this real-time feedback system was able to reliably and accurately position the aircraft at specific altitudes with observed precision of +/- 0.6 m. These precision metrics were true for the X and Y directions as well.

Weather Data System

The weather measurement system consisted of a winch-controlled, helium-filled balloon, sensor/telemetry package and a ground based receiver connected to a computer for control and data storage. The balloon and sensor package were systematically raised and lowered from ground level to about 153 m to obtain weather data as a function of altitude. The system stored averaged measurements of pressure-altitude, pressure, relative humidity, temperature (wet bulb and dry bulb), wind speed and direction with a time stamp at 10 second intervals. These parameters allowed the accurate estimation of air density and the speed of sound for prediction purposes and a real-time update of wind values and inversion layers conditions during the test. The density and speed of sound estimates were later averaged as a function of altitude.

Acoustic Instrumentation

The acoustic instrumentation consisted of a twelve-microphone array which was in the shape of a semi-circle (Fig. 1). The microphones were omnidirectional 1/2-inch condenser type (B&K 4134S) having a frequency response of 0.01-40,000 Hz with a maximum sound pressure level of 160 dB. The microphones were secured to 1 m square ground boards after being mounted with 3-inch foam windscreens.

The signals from the twelve microphone systems (microphone, preamp and adapter) were recorded on a Honeywell 101 FM instrumentation recorder at a tape speed of 15 inches per second. This record rate resulted in a dynamic range of 48 dB and a data bandwidth of 50 kHz for each of the signals.

Microphone calibrations were performed with a piston acoustic calibrator at the beginning and end of each daily test period. White noise injections were also performed to assess the specific microphones frequency response variability. Ambient noise levels were recorded before and after each test and if possible for short periods within the test phase. This was possible several times when the XV-15 was required to power down for safety checks.

The analog acoustic data tapes were returned to NASA Langley for processing on the Acoustics Division Data Reduction and Analysis System (ADDRAS, Ref. 4). The ADDRAS was used to perform acoustic signal calibration, data stream selection, anti-alias filtering, digitization, engineering units conversion, display and storage.

Operating Procedures

The test operating conditions included several values of rotor RPM, gross weight and altitude. All altitudes reported here are referenced to the rotor disk heights with the nacelle angles set to 90 degrees. Each hover test point required a sampling period with the vehicle heading at two values 180 degrees apart to collect the full circumferential acoustics. Once a specific rotor RPM was established and the aircraft was directed to location by the positioning system, data from the microphone array were recorded by the acoustic instrumentation system for 30 seconds.

The aircraft demonstrated precision handling qualities during the hover test. Only at the 156 m altitude hover condition was vehicle position movement of concern.

Aircraft gross weight was not controlled but was constantly monitored and recorded. A knowledge of fuel consumption rates as a function of power setting/duration and the initial aircraft weight allowed a time dependent determination of aircraft gross weight. Changes in gross weight during the test period were observed to be approximately -21 pounds per minute; at 589 RPM; at altitudes above ground effect conditions and below 152.4 m.

A polar coordinate reference system was used which has its origin exactly between the two rotor system hubs (with nacelle tilt at 90 degrees; helicopter mode). The origin is a point on the reference plane which is defined to be coplanar with the two rotor disks' tip path planes (Fig. 2). Each of these planes are assumed parallel to the ground for the hover condition.

Data presented here are from eight 30 second flights representing four altitudes, eight aircraft weights having a mean of 13161 pounds and standard deviation of 206 pounds at constant RPM of 589 (rotor tip speed; 235 m/s). Table 1 lists the flight conditions for these test points. A more detailed description of the hover test and acoustic results is presented by Conner and Wellman (Ref. 5).

XV-15 Tiltrotor Aircraft

The XV-15 aircraft (Fig. 3) is a 13,000 pound (design gross weight) proof of concept research vehicle for tiltrotor technology. It was designed to display generic tiltrotor characteristics with respect to performance and acoustics. The aircraft has 7.62-m-diameter 3-bladed rotors on tiltable nacelles which are wing-tip mounted. The tiltable rotor systems allow vertical, helicopter similar, liftoff/hover and transition to airplane mode for higher cruise speeds. During this transition the lifting surface changes from the rotating blades to a combination of the rotating blades and wing to all wing. Further details are given in Reference 6.

In the mid-eighties, to accommodate aircraft gross weight increases and to increase performance in the hover and tiltrotor modes, the composite ATB were designed and fitted to the XV-15 (Ref. 3). The composite materials allowed greater design flexibility to include nonuniform taper, 43 degrees of non-linear twist and detachable tips and cuffs. This design resulted in blades that have a solidity of 0.103.

During the hover tests, the basic cuff and basic tips were fitted to the blades. For all flights, the wing flaps were positioned fully downward to reduce wing download. The rotor systems were set to be in phase; angular offset between the two rotor systems was 0 degrees. The two nacelle housed engines were mechanically connected and produced similar

operating speeds of 589 RPM. This produced an acoustic blade passage frequency of 29.45 Hz, tip speed of 235 m/s and a nominal hover tip Mach number of 0.69. The nominal disc loading is 13.2 pounds per square foot relative to the design gross weight.

Theoretical Setup

Fountain Model

The fountain effect model presented by Coffen and George is an aerodynamics model to simulate the effect of the fountain/recirculation flow on blade loading. It is a first approximation model. The results of this model are used in conjunction with the aeroacoustic code, WOPWOP (Ref. 7), developed at NASA Langley, that predicts the discrete frequency noise of helicopter rotors by employing Farassat and Succi's most advanced subsonic acoustic formulation (Ref. 8). The code allows for realistic helicopter blade geometry, motions and aerodynamic loadings which are input by the user. The accuracy of the acoustic results reflects the fidelity of the input provided.

The rotor geometry for the ATB blades on the XV-15 were defined from data provided by Boeing Helicopter Company and general blade information from Reference 6. The actual time varying blade loadings for a hovering tiltrotor have not been well defined and are the subject of ongoing investigation. Thus some assumptions have been made in developing the loading model used in these WOPWOP calculations. For the fountain effect aerodynamics model, the blade motions were assumed to be unaffected by the recirculation/fountain effect for the hover case; ie, the flapping, feathering, and lagging degrees of freedom are assumed to be azimuthally constant.

As the exact nature of the fountain flow and its effect on the rotor blade loading is not known, a mathematical model was developed to simulate this phenomenon by introducing a deficit in the inflow velocity over the wing. The parameters of the model are based on the chord of the wing and an empirical deficit quantity. The main effect of the inflow velocity deficit is to increase the angle of attack of a blade element as it sweeps over the wing, that results in a time varying blade loading and thus produces sound.

The mathematical model, based on flow visualization tests, defines the width of the affected region to be 4/5 of the wing chord with an inflow velocity deficit of 20%. A sketch of the inflow velocity profile near this region is shown in Figure 4. As the blade approaches the region over the wing, the inflow is made to decrease as a quarter sine wave to 80% of the constant inflow velocity calculated from momentum theory. The inflow profile is symmetric about the mid-chord point of the wing. The forward sweep of the wing is not accounted for. Figure 5 depicts differential pressures as a function of azimuthal station showing the effect of the quasi-steady model of reference 2 on blade surface pressures as a blade sweeps over the wing (wing center station; 270 deg). The three curves are typical pressure changes at three example spanwise locations. The model used twenty-five spanwise locations for the acoustic calculations. Twenty-five leading edge and twenty trailing edge chordwise locations were used to model the blade lower and upper surfaces.

The fountain effect model is approximate and is currently substantiated only by flow visualization experiments. It simulates an idealized flow disturbance caused by the wing obstructing the downwash. Further investigation into the recirculating/fountain effect will provide more accurate models in the future.

Blade Loading Distribution

As user input, WOPWOP requires the pressure on the blade surface as a function of azimuth, radial station and chordwise position. This problem can be quite complex for a rotor in forward flight, while the hovering case is simpler. The problem lends itself to a 2-D blade element simplification. The loading characteristics of each radial station are calculated as if for a 2-D airfoil in a steady flow. Lift and drag were interpolated from airfoil specific data provided by Boeing. These data represented measured results for the specific airfoils as a function of Mach number and angle of attack for steady 2-d flow.

Modelling an accurate quasi-steady chordwise pressure distribution on the ATB blades is a more complicated problem considering the variables involved in the process: rotor thrust, inflow conditions (attached or separated), geometric angle of attack, rotor tip Mach number, etc. For standard NACA airfoils, the steady chordwise pressure distribution can be approximated using the velocity addition method of Abbott and Von Doenhoff (Ref. 9). This method is accurate for slender airfoils at small angles of attack (fully attached flow) and low Mach numbers. The ATB blades are not standard NACA airfoils and in order to use accurate chordwise pressure distributions, one would have to rely on experimental data or CFD results. As neither of these alternatives exist, the chordwise loading was modelled using a triangular loading

distribution. This simplification was based on the premise that the loading distributions are approximately acoustically compact.

There are two conditions for acoustic compactness given by Farassat (Ref. 10). One is that the distance from the source to observer should be much greater than the length scale of the source. Using a collapsing sphere analysis, the time taken for a sphere, collapsing on the observer at the rate of M=1, to cross the acoustic source should be much less than the period of the acoustic pressure fluctuation. This implies the following compact limit:

$$r_{obs} >> \text{chord}$$

$$\text{chord}/((1.-M_{tip})*c) << 1/\text{frequency}.$$

To arrive at an upper limit for frequency for the XV-15 in hover, use the following values: M_{tip} =0.65, the chord at 90% radius = 0.34 meters, and assume a speed of sound of 340 m/s. This implies that the accuracy of the chordwise pressure distribution is unimportant for frequencies less than 350 Hz for the "worst case" calculation. One should note that the blade tapers towards the tip. Also the relative Mach number decreases inboard of the tip and at all observer locations not directly behind the aircraft and inplane with the rotors. Thus, most cases will be accurate to significantly higher frequencies.

The compactness assumption was tested by comparing the WOPWOP calculations of three different chordwise distributions for the XV-15 (single rotor calculation) using the standard metal blades which employ NACA 64 series airfoils. The three distributions were constant chordwise loading, a triangular loading distribution where the maximum pressure occurred at the 1% chord point, and a chordwise accurate pressure distribution calculated using the velocity addition method of Abbott and Von Doenhoff. The total lift on each blade element was the same for the three loading distributions. A near in plane observer location to the rear of the aircraft (θ=-11, ψ=0) was chosen so as to maximize the acoustic directivity effect due to the Mach number of the blade as it passed through the fountain moving towards the observer. The results of these calculations are shown in Figures 6 and 7. The spectra are very close out to about 800 Hz (Figure 7, Harmonic number: 28) where the constant chordwise loading method deviates significantly. The triangular loading distribution is shown to be a valid and accurate simplification as it never varies from the velocity addition technique results by more than a few dB throughout the spectrum. Also note that the OASPL differs by less than an half a dB for the triangular loading and chordwise accurate loading cases.

Operational Procedures

Two WOPWOP runs were performed for each observer location predicted to account for the two rotor systems on the XV-15. Because WOPWOP does not conveniently allow clockwise rotating (from above) rotor systems, a mirror image scheme was used. The results of each run were then summed to give the total far-field prediction. The summed pressures were then doubled to correct the free-field prediction to a hard surface estimate.

When performing the predictions, weather data derived parameters were used as input to WOPWOP. Table 2 lists the altitude dependent averaged derived data.

In the predictions, in addition to adjusting the collective to account for the different air densities at altitude the rotor lift was set at 111% of aircraft weight to approximately account for the wing download.

Results

Environmental

The ambient noise OASPL levels were at least 20 dB below the lowest XV-15 hover acoustic data with the majority of the acoustic energy at frequencies below 200 Hz. The windspeeds associated with the eight flights presented here were low with a mean of 0.9 m/s and standard deviation of 0.7 m/s with variable direction. The windspeed variability was associated with altitude being lowest at ground level and reaching a maximum at 135 m. No temperature inversion conditions were observed during this test period.

Experimental Acoustic Directivity

The spherically corrected (to 57.2 rotor diameters) acoustic time histories show distinct side-to-side and fore-aft symmetry relationships. Figures 8-11 show the circumferential pressure time histories for the polar angles measured (θ= -7.1, -12.6, -23.0 and -45.7).

Similar trends in side-to-side symmetry are evident at each of the polar angles. The amplitudes and periods are similar for each side-to-side comparison. At the rear there is less side-to-side symmetry, including differences in spike

amplitude, timing and frequency content. This is due to the side-to-side differences in the unsteady, asymmetric fountain flow which dominate rearward sound radiation. (The fountain unsteadiness is discussed in reference 11).

Fore-aft asymmetry is the most striking trend present in these data. With respect to the long period (low frequency) loading and thickness associated noise, there is an azimuthal dependent amplitude and period modulation evident in the forward data. This is seen in the time domain data of Figure 8 (for example) at three azimuthal stations (ψ=150,165,180). The characteristic periods of the time domain data are longer at ψ=150 and 180 relative to the periods observed at ψ=165. Also the amplitudes of the acoustic data at ψ=165 is lower than the amplitudes at ψ=165 and 180. This observed period and amplitude modulation is associated with interference pattern effects resulting from the two rotor systems. (For frequency domain integrated metric summaries of this phenomenon refer to Reference 5.) More specifically, this is due to the varying differences in the source-receiver path length and varying Doppler effects of the rotating acoustic sources of the two rotors. This modulation is distinct in the acoustic data associated with the three shallow polar angles but not so at θ = -45.7. With respect to long period and amplitude character, the entire set of time histories for θ = -45.7 is difficult to interpret because of the presence of broadband noise.

A different type of amplitude modulation appears in the rear acoustic data (for example Figure 11). This trend applies to the high amplitude spikes and the lower amplitude thickness and loading components found in the rear acoustics. The general trend is for the amplitudes to be smallest at the sides (ψ = 90 and 270) and have a maximum directly behind the aircraft (ψ = 0).

The presence of the short duration, high amplitude spikes is another difference between the fore and aft acoustics. In the data associated with the three shallow polar angles, the spikes are only found in the aft acoustics. The data associated with θ = -45.7 has observable spikes in the forward area but they are much smaller than those in the rear stations. The fore-aft and polar angle dependence of these spikes are shown in Figure 12. The spikes do not occur in the forward acoustic data but are present in all of the rear data. These spikes are due to the rapid change in lift as the blades pass through the varying inflow over the wing. The resulting sound is preferentially radiated to the rear of the aircraft due to the Doppler amplification effect. This radiation directivity is similar to BVI radiation directivity because both are dipole acoustic sources. At θ = -45.7 the spike amplitudes are approximately three times larger than the amplitudes at the other polar angles. Spike amplitude variability as a function of time is also observed at all polar angles. This is also due to the unsteadiness in the actual fountain flow.

Theoretical Acoustic Directivity

The WOPWOP output is a time dependent pressure fluctuation for a single blade passage. For comparison purposes, these data were repeated and concatenated to produce multiple blade passages as in the experimental data. The side-to-side symmetry comparisons for the predicted data are inappropriate because they are theoretically identical using the present model.

The fore-aft symmetry relations are subject for comparison. Figure 13 shows theoretical time domain data for the conditions associated with θ = -45.7. With respect to amplification modulation, the rear acoustic data is similar to the experimental data (Fig. 11). The spike pulses are at a minimum at the sides and grow to a maximum at the rear. The theoretical long period (thickness and loading) components are modulated similarly. At θ = -45.7, the theoretical data shows the spike phenomenon present in the fore and aft acoustic data, being of higher amplitude in the rear relative to the forward data. The theoretical data spikes always appear with equal positive and negative pressure contributions.

The predicted fore-aft and polar dependence of the acoustic data are shown in Figure 14. General trends in spike amplitude relative to the aircraft's front and rear acoustics are similar to the experimental data (Fig. 12). In the predicted forward acoustic data, the spike phenomenon is present at the three deeper polar angles (θ= -12.3, -23.0, -45.7) although the amplitudes are small relative to the associated rear acoustic amplitudes. Such spikes are not observed on the forward experimental data. In the rear acoustics, as with the experimental data (Fig. 12), the amplitudes of the spikes at θ = -45.7 are much larger than the amplitudes at the shallow polar angles.

The location of the spikes in the predicted and experimental data relative to the long period loading and thickness noise components is shown in Figure 15. The spike perturbations in both the time series systematically occur at the same time relative to the longer period pressure fluctuations. In both

the data sets, the low frequency loading noise component takes approximately 22 milliseconds to transition from its minimum to its maximum. About twelve milliseconds are required to go from the maximum back to the next minimum. These two time segments when summed make up one blade passage period. The spike perturbation systematically occurs during the latter part of the maximum to minimum transition.

The dashed line segments located on the long period components of the predicted time series of Figure 15 represent the WOPWOP prediction for these time periods for the same aircraft conditions with the fountain model removed from the calculations. The spiked pressure fluctuation is associated with the fountain effect mechanism. These results suggest the spikes observed in the experimental data are similarly due to the fountain effect noise mechanism. These results are not specific to these particular θ and ψ positions but are representative of other θ,ψ combinations tested.

Discussion

The relative timing and magnitudes of the acoustic spikes in the predicted and experimental data suggest they arise from the same mechanism; the fountain effect. Experience with conventional helicopter noise mechanisms suggest that these conventional mechanisms are unlikely to produce pressure fluctuations of such duration and amplitude when in the hover condition. The character of these spikes might reasonably suggest a near-parallel BVI situation, but these are not generally observed in hover aerodynamics because the downwash sufficiently displaces the shed vortices so as to prevent it and the tip vortices are essentially perpendicular to the blades. The general agreement in directivity comparisons between the predicted data with the fountain effect model and these experimental data also support the fountain mechanism. In the future, this result can be more rigorously tested by acoustic triangulation techniques to identify the location of the spikes' origins, relative to the disk planes of the tiltrotor.

The fountain effect noise mechanism produces far-field spike-like pressure fluctuations which have directivity patterns that show increased amplitude in the rear of the tiltrotor with a region of increased amplitudes 45 degrees below the disk planes as one would expect from an unsteady lift dipole sound source. These pressure fluctuations are at a minimum on the tiltrotor's sides and increase to a maximum directly behind and below the aircraft. The hover acoustics test did not allow a full mapping of the fountain effect noise directivity because lower polar directivity associated acoustic data are needed. The present test revealed this fact. Additional far-field acoustic measurements using a wider range of polar angles are needed to fully map the fountain effect acoustic directivity.

The modulation effects observed in the front of the tiltrotor are believed to be a result of the interference patterns resulting from the two rotor systems. Resulting from different source to observer geometries associated with the two rotors and a single observer, the source signals have relative phase differences when summed in the far-field. This can produce the observed period and amplitude modulation that was observed in the data. These effects are not believed to be associated with the fountain effect mechanism.

The variability of the experimental data relative to the predicted results suggest the fountain/recirculation phenomenon is dynamic with some long timescales (relative to acoustic timescales). The observed side-to-side variability may be associated with fountain/recirculation aerodynamics which vary slowly relative to acoustic timescales. These observations could conceivably be associated with the tiltrotor's stability during the hover tests but recent scale model flow visualization studies at Cornell University show similar random side-to-side fluctuations in the recirculation flow. The flow visualization study on a 1/12 scale tiltrotor showed the fountain flow dynamics to be unsteady and to randomly move from disk to disk. The extrapolation of this character to the hovering XV-15 could result in associated side-to-side variations in the far-field acoustics. The two independent experimental results corroborate each other.

The theoretical model proved useful in predicting and identifying the acoustic fountain effect character in the experimental data. It predicted the large trends correctly but failed to simulate side-to-side (longer timescale, dynamic) characteristics. The waveform shape differences between the predicted and experimental data are related to the differences in complexity of the real world aerodynamics and those modelled. Refinements in the fountain effect acoustic model will only follow a better understanding of the local aerodynamics associated with the tiltrotor aircraft.

The observation of multiple spikes as observed in the experimental data (Fig. 11, ψ = 30, 45, θ= -45.7) shows that the current fountain model does not encompass all of the physical phenomena. Detailed aerodynamics modelling

combined with much needed aerodynamic experimental studies and experiments using pressure instrumented blades may clarify this conceptual model in the future.

Conclusions

Noise mechanisms and directivity patterns which are unique to tiltrotor aircraft were studied. They result from tiltrotor-specific aerodynamics which mainly occur in hover mode. The "fountain effect" noise mechanism produces distinct time domain pressure fluctuations, and azimuthal amplitude variations due to phasing and Doppler differences between the two rotors. Acoustic measurements from a full-scale XV-15 tiltrotor with the advanced technology blades are presented which show the nature and directionality of tiltrotor noise. Predicted acoustic directivity results are also presented which show agreement with the measured data. The aeroacoustic code, WOPWOP, was used in conjunction with a mathematical model which simulated an idealized fountain/recirculation aerodynamic effect on the rotor's blade surface pressures. The model simulated the fountain flow by introducing a deficit in the inflow velocity over the wings and used quasi-steady aerodynamics to evaluate lift changes. The predictions were used to identify the spike character in the measured data as fountain effect associated noise. The directivity of the fountain effect noise was observed to be dominant at the rear of the aircraft with increased intensities 45 degrees below the rotor disk planes. Future aerodynamic studies are warranted to increase the understanding of the fountain/recirculation flow and to evolve a more accurate mathematical model.

Acknowledgements

This work was supported by NASA Langley Contract NAS1-19000 and by NASA Ames Grant NAG 2-554.

References

1. McVeigh, Michael A.: Grauer, William K.: and Paisley, David J.: Rotor/Airframe Interactions on Tiltrotor Aircraft. 44th Annual Forum Proceedings of the American Helicopter Society, Washington, D.C., June 1988.

2. Coffen, Charles D.: and George, Albert R.: Analysis and Prediction of Tilt Rotor Discrete Frequency Noise. 46th Annual Forum Proceedings of the American Helicopter Society, Washington, D.C., May 1990.

3. Alexander, Harold R.: Maisel, Martin D.: and Giulianetti, Demo J.: The Development of Advanced Technology Blades for Tilt Rotor Aircraft. Vertica Vol. 10, No. 3/4, pp. 315-339, 1986.

4. Becker, Lawrence E.: Rutledge, Charles K.: Smith, Rita A.: Grandle, Robert E.: and Golub,Robert A.: ADDRAS - An Integrated Systems Approach from Experimental Design to Data Analysis. Proceedings of the American Helicopter Society's Technical Specialists Meeting on Rotorcraft Acoustics and Fluid Dynamics. October, 1991.

5. Conner, David A.: and Wellman, Brent .: Far-Field Hover Acoustics of the XV-15 Tiltrotor Aircraft with Advanced Technology Blades. Proceedings of the American Helicopter Society's Technical Specialists Meeting on Rotorcraft Acoustics and Fluid Dynamics. October, 1991.

6. Maisel, Martin D.: ARMY/NASA XV-15 Tilt Rotor Research Aircraft Familiarization Document. NASA TM X-62, 407, January, 1975.

7. Brentner, Kenneth S.: Prediction of Helicopter Rotor Discrete Frequency Noise, A Computer Program Incorporating Realistic Blade Motions and Advanced Acoustic Formulation. NASA TM 87721, October 1986.

8. Farassat, F.: and Succi, G. P.: The Prediction of Helicopter Rotor Discrete Frequency Noise. Vertica, vol. 7, No. 4, pp. 309-320.

9. Abbot, Ira H.: and Von Doenhoff, Albert E.: Theory of Wing Sections. Dover Publications Inc., New York 1959.

10. Farassat , F.: Linear Acoustic Formulas for Calculation of Rotating Blade Noise. AIAA Journal Vol. 19, No. 9, pp. 1122-1130, September 1981.

11. Coffen, Charles D.: George, Albert R.: Harding, Hal: and Stevenson, Ryan: Flow Visualization and Measurements of a 1/12 Scale Tiltrotor Aircraft in Hover. Proceedings of the American Helicopter Society's Technical Specialists Meeting on Rotorcraft Acoustics and Fluid Dynamics. October, 1991.

Table 1. Hover test flight conditions* and resulting geometry.

FLIGHT	ALTITUDE ** (m)	GROSS WEIGHT (lbs)	HEADING *** (deg)	NOMINAL θ (deg)	NOMINAL r/R
1	18.9	13469	140	-7.1	40.1
2	18.9	13498	320	-7.1	40.1
3	34.1	13140	140	-12.6	41.1
4	34.1	13108	320	-12.6	41.1
5	64.6	13071	140	-23.0	43.4
6	64.6	13041	320	-23.0	43.4
7	156.1	12696	140	-45.7	57.2
8	156.1	12998	320	-45.7	57.2

* all flights 589 RPM
** relative to disk plane
*** heading of 140 degrees; rear acoustics sampled
heading of 320 degrees; forward acoustics sampled

Table 2. Altitude dependent derived variables from weather data.

ALTITUDE (m)	POLAR DIRECTIVITY θ (deg)	DENSITY ρ (kg/m^3)	SPEED OF SOUND c (m/s)
18.9	-7.1	1.2774	335.32
34.1	-12.6	1.2744	334.45
64.6	-23.0	1.2686	333.99
156.1	-45.7	1.2564	333.77

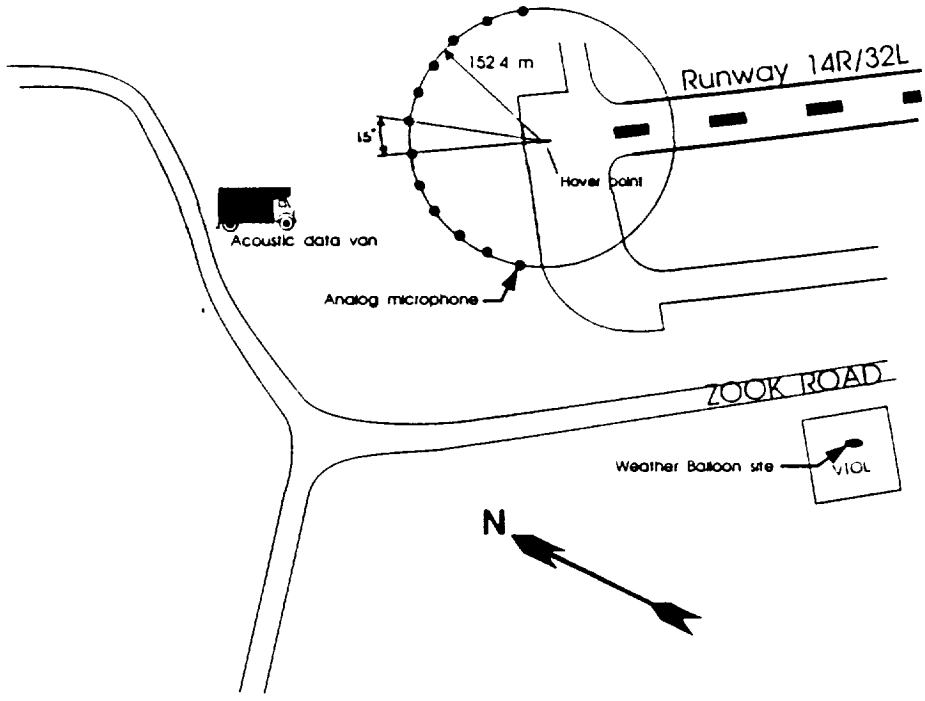

Figure 1. Moffett Field test area.

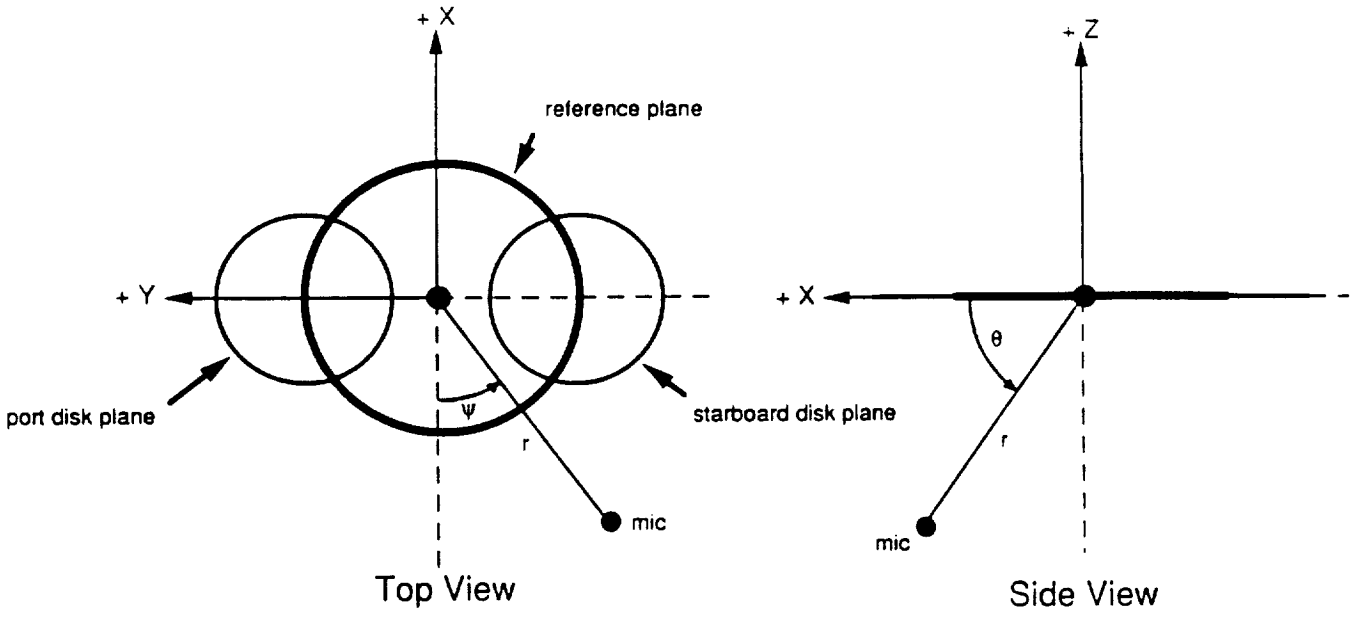

Figure 2. Geometry of coordinate system.

Figure 3. XV-15 Tiltrotor in Hover Mode.

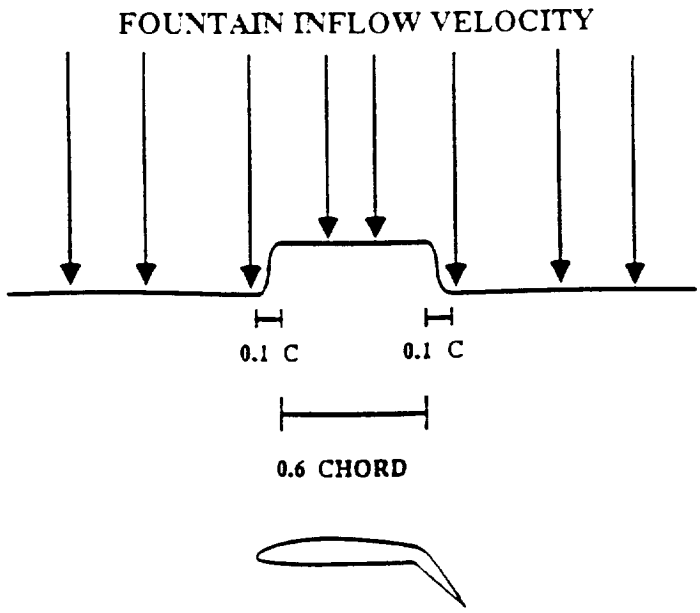

Figure 4. Schematic of Velocity Deficit due to Fountain Effect.

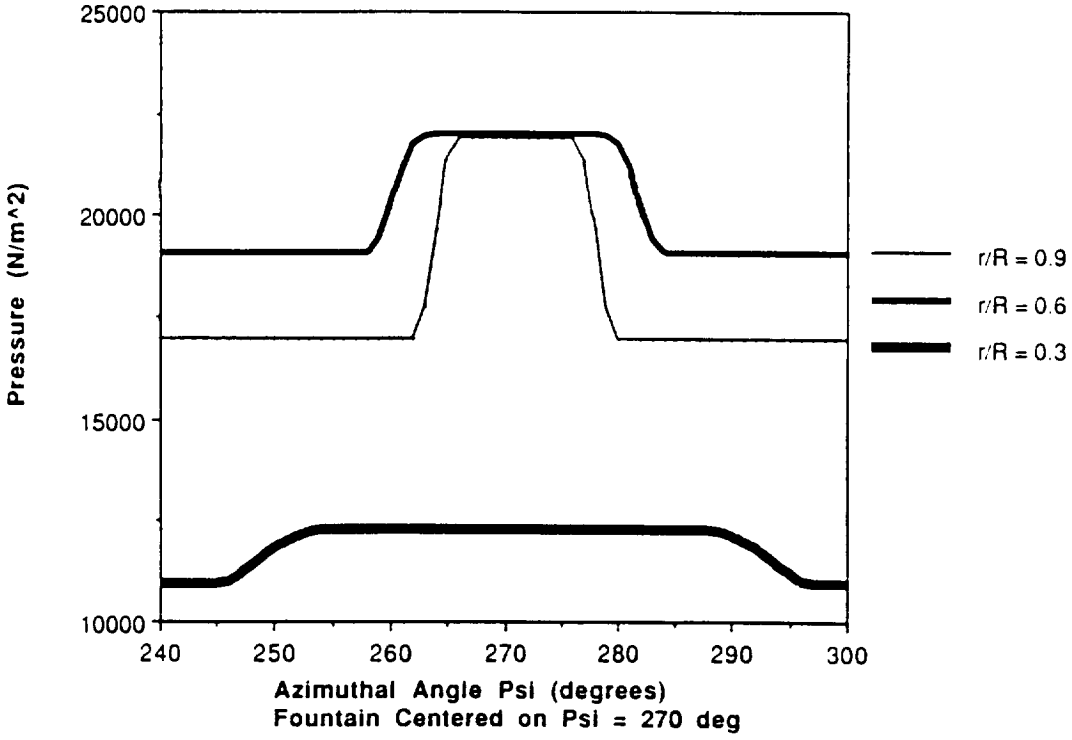

Figure 5. Fountain Model Results of Differential Pressure at 25% Chord for Three Example Radial Stations.

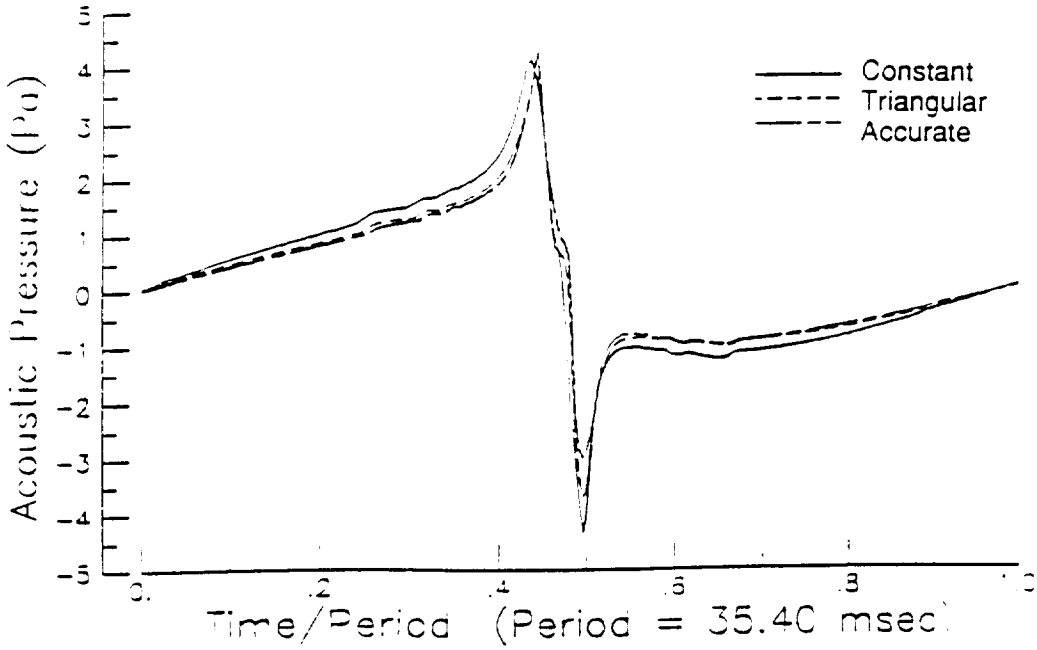

Figure 6. Results from Chordwise Loading Distribution Comparisons.
Waveform of sound for XV-15 Hover Case (single rotor).
(θ= -11, ψ=0, r= 61 m)

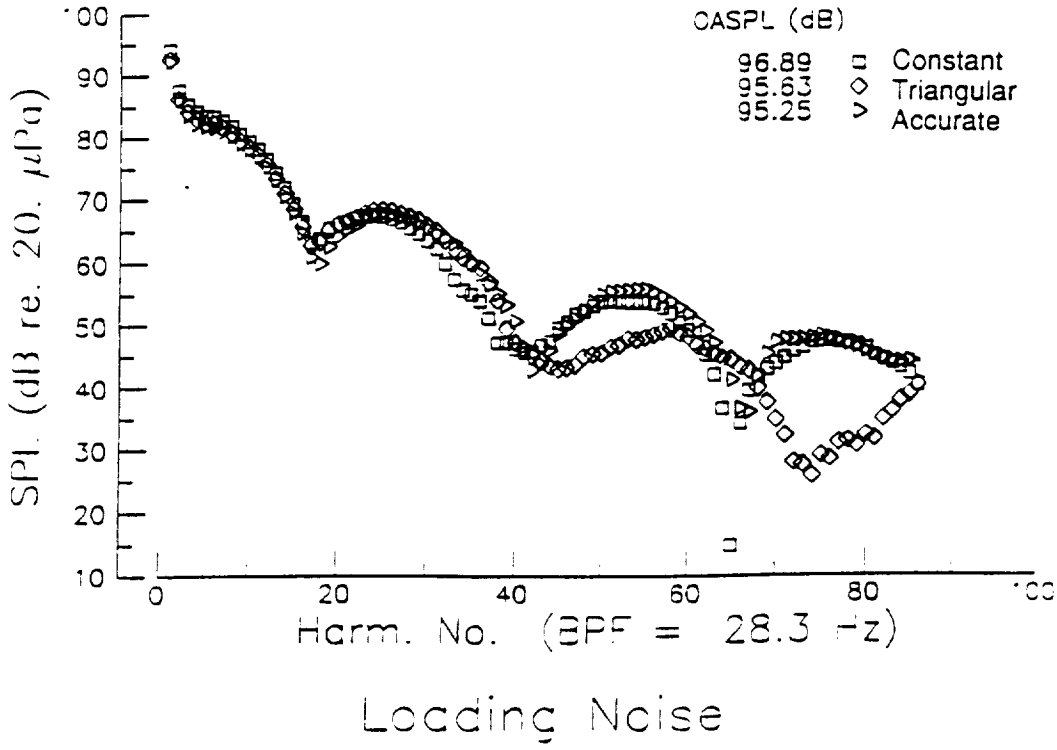

Figure 7. Results from Chordwise Loading Distribution Comparisons.
Spectra of sound for XV-15 Hover Case (single rotor).
(θ= -11, ψ=0, r= 61 m)

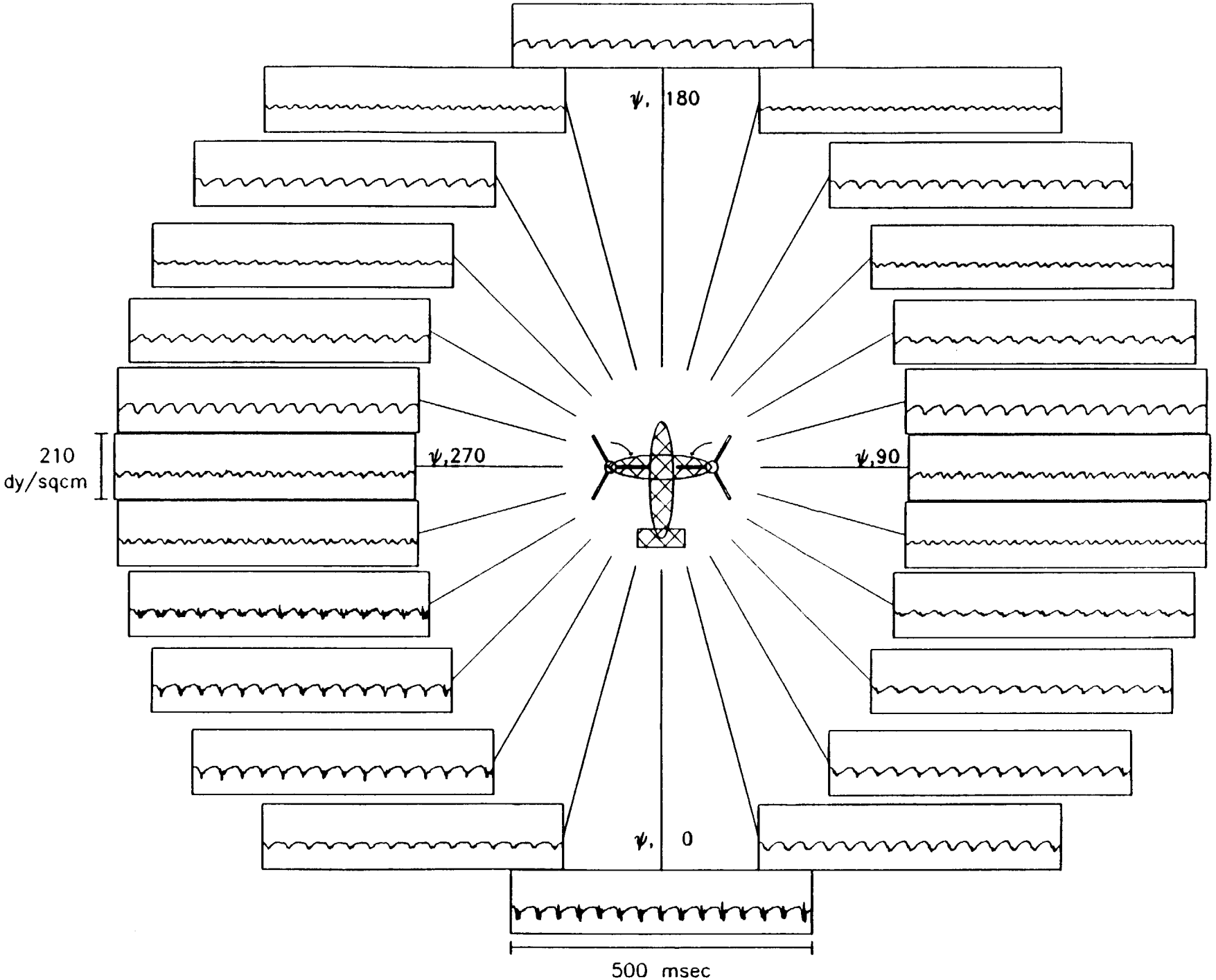

Figure 8. Experimental acoustic time domain data (θ = -7.1).

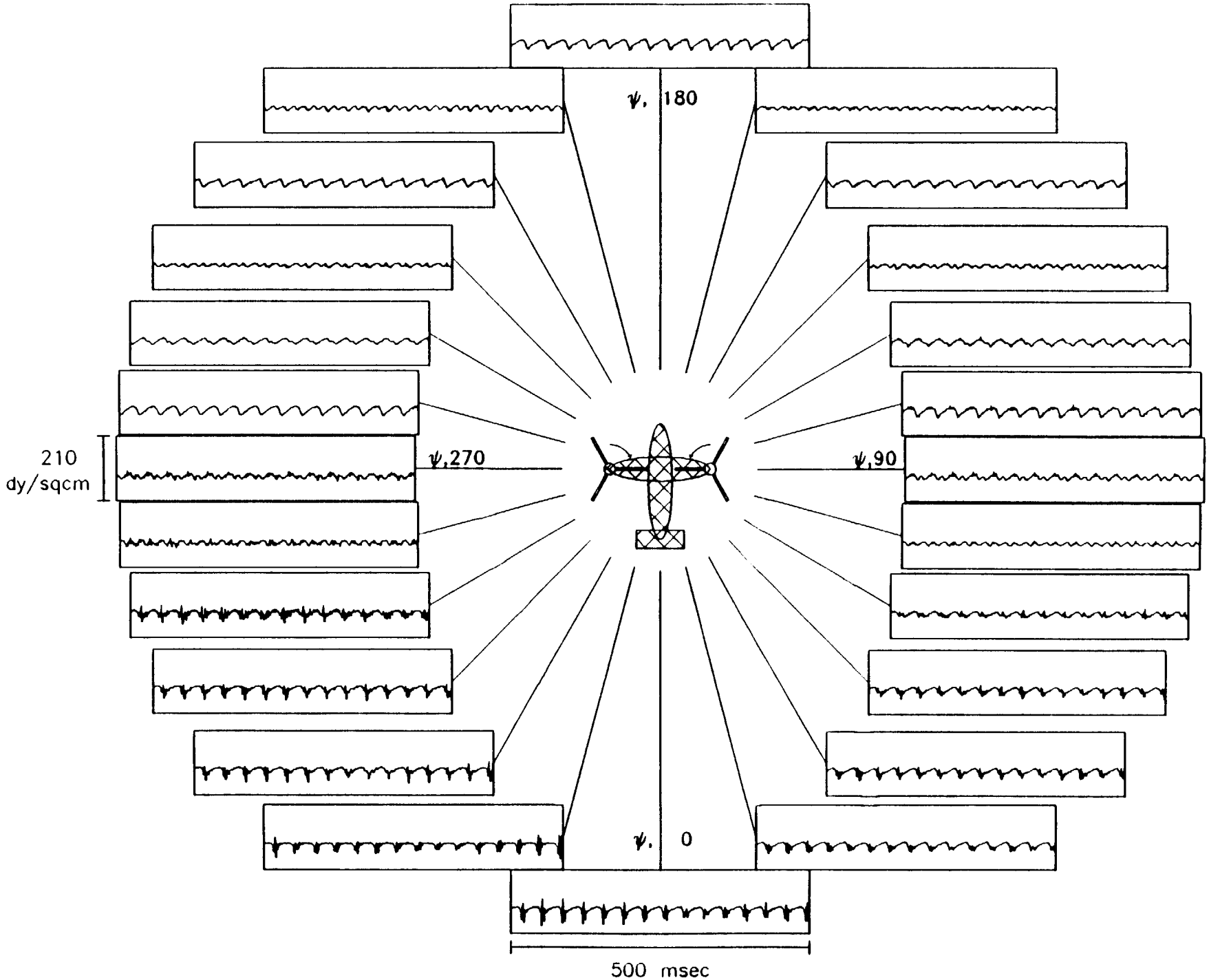

Figure 9. Experimental acoustic time domain data ($\Theta = -12.6$).

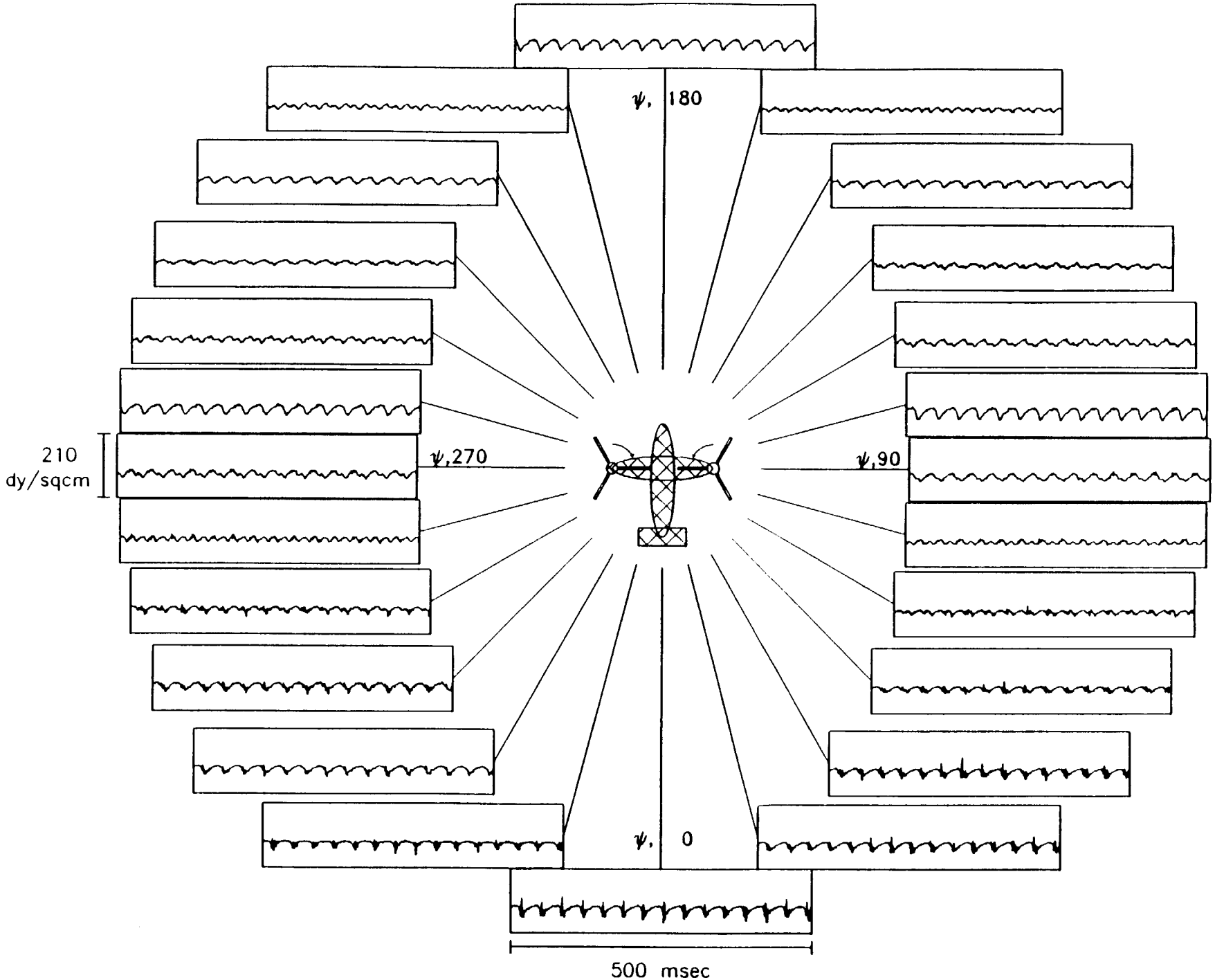

Figure 10. Experimental acoustic time domain data (θ = −23.0).

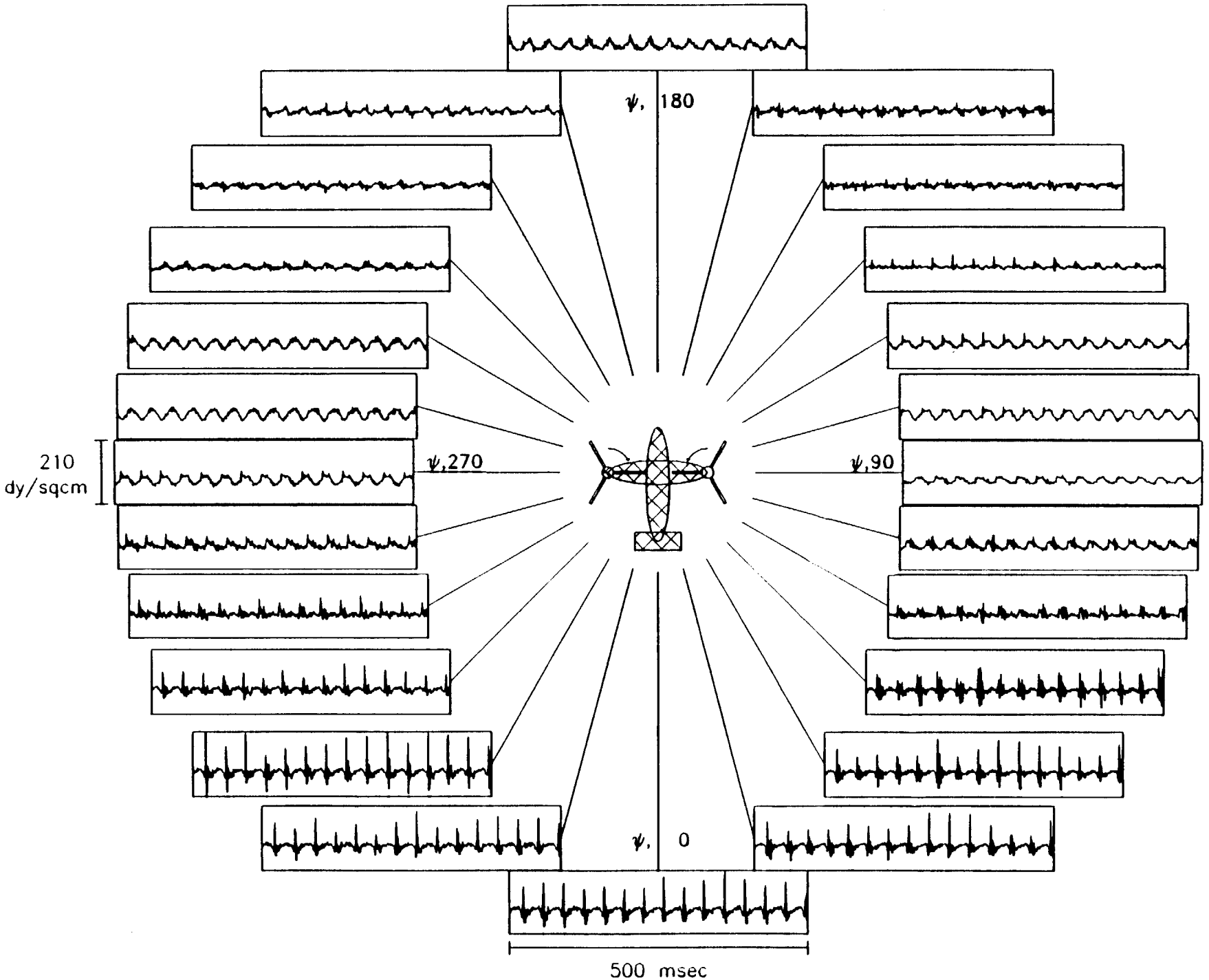

Figure 11. Experimental acoustic time domain data (Θ = -45.7).

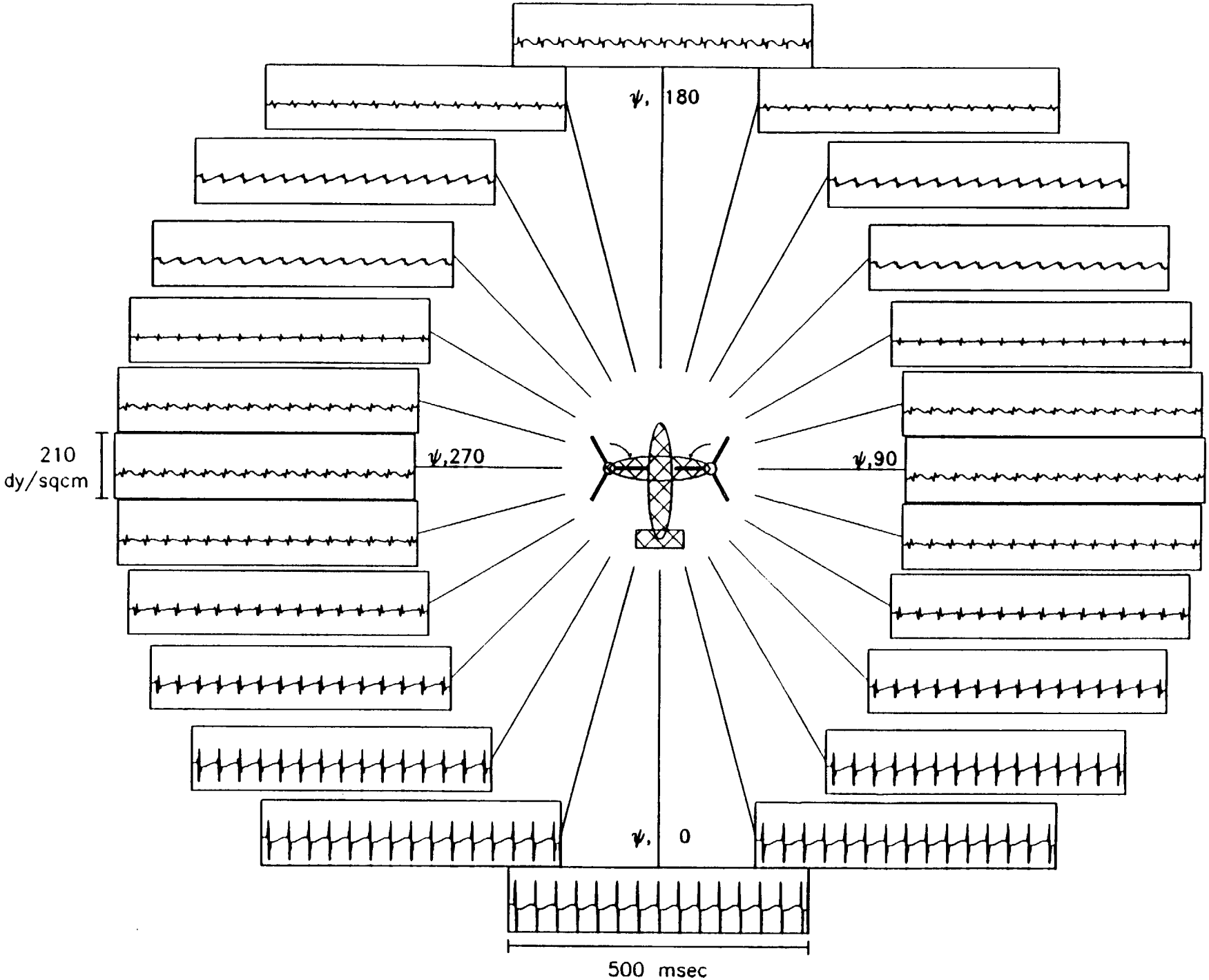

Figure 13. Predicted acoustic time domain data (Θ = -45.7).

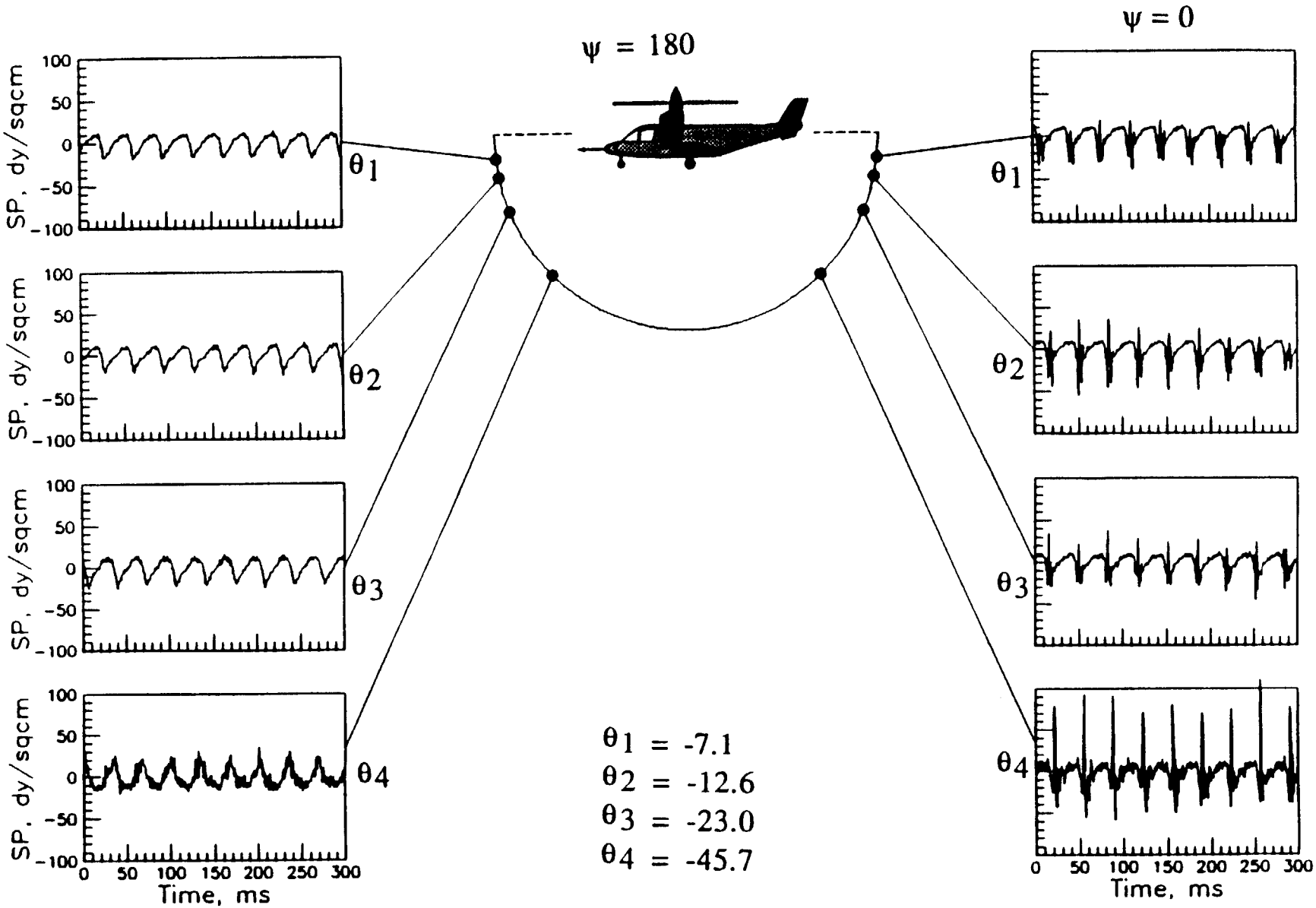

Figure 12. Fore/aft/polar measured acoustic time domain data.

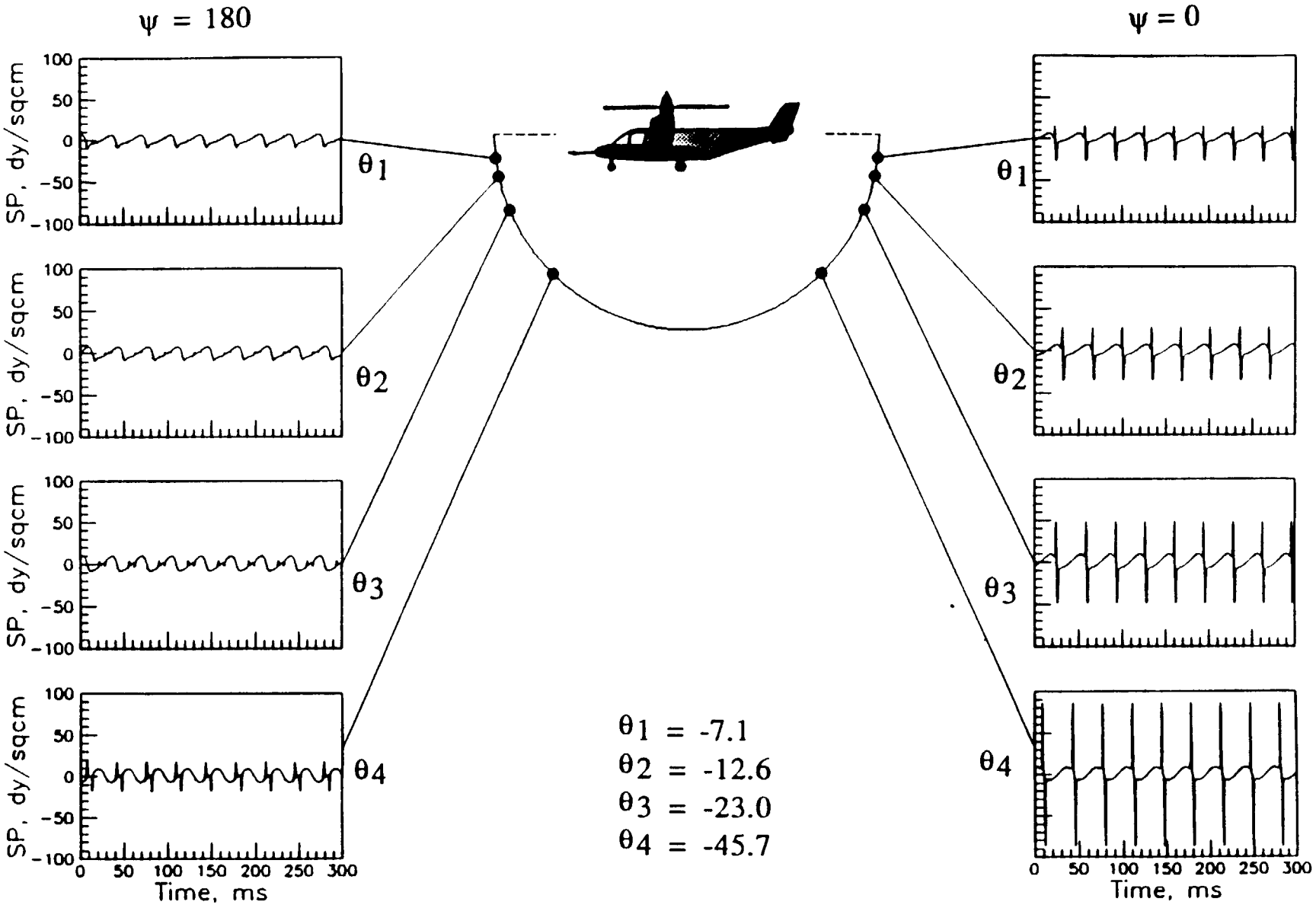

Figure 14. Fore/aft/polar predicted acoustic time domain data.

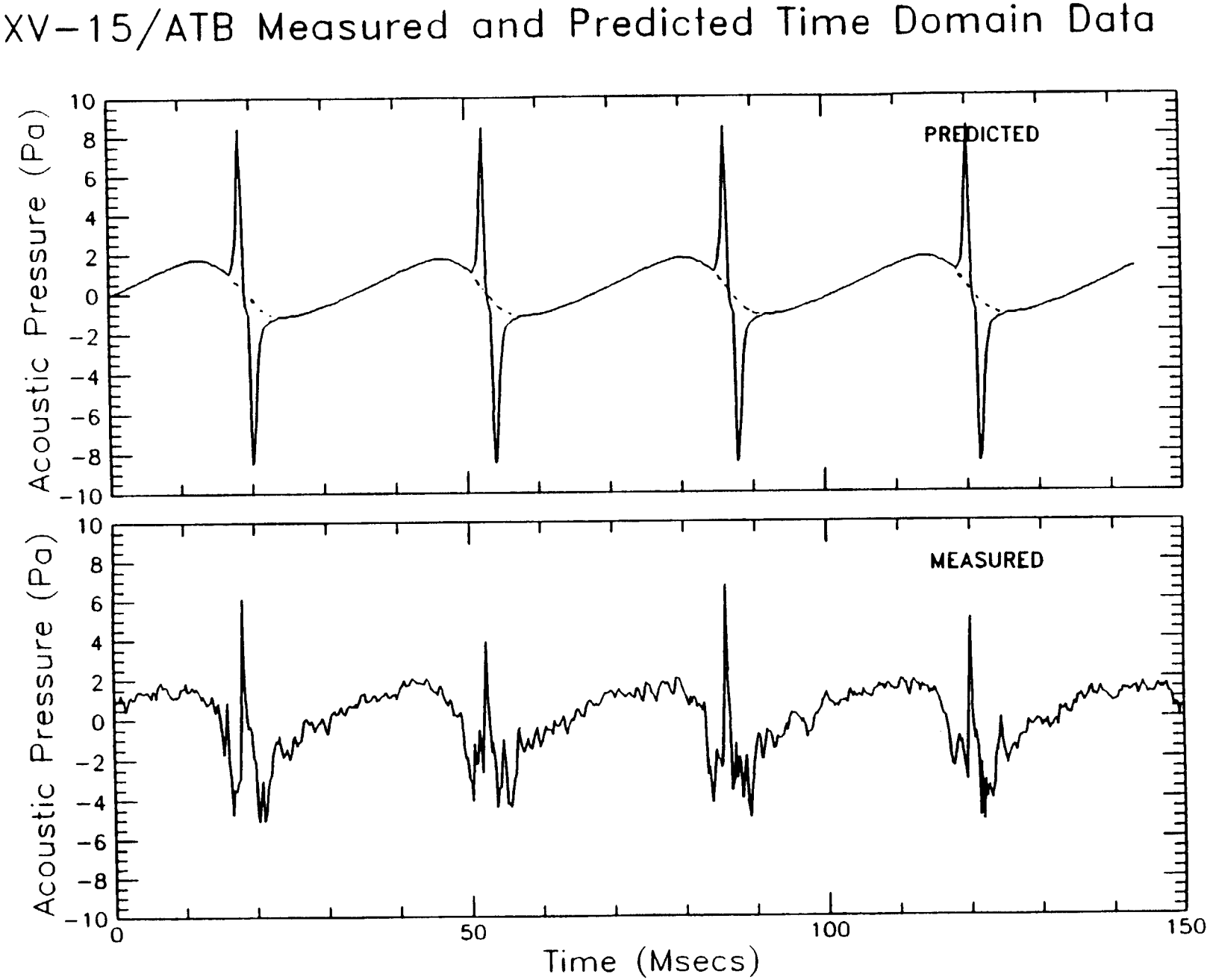

Figure 15. Experimental and predicted acoustic time domain data (ψ=0, θ=-23).